frontiers | Frontiers in Physics

ORIGINAL RESEARCH
published: 27 April 2022
doi: 10.3389/fphy.2022.880689

Dynamics of Ring-Cleavage Reactions in Temozolomide Induced by Low-Energy Electron Attachment

Eugene Arthur-Baidoo[1,2], Farhad Izadi[1,2], Carlos Guerra[3], Gustavo Garcia[3], Milan Ončák[1] and Stephan Denifl[1,2]**

[1]*Institut für Ionenphysik und Angewandte Physik, Leopold-Franzens Universität Innsbruck, Innsbruck, Austria,* [2]*Center for Molecular Biosciences Innsbruck, Universität Innsbruck, Innsbruck, Austria,* [3]*Instituto de Física Fundamental, Consejo Superior de Investigaciones Científicas, Madrid, Spain*

We have used a crossed electron molecular beam setup to investigate the behavior of the anticancer drug temozolomide (TMZ) upon the attachment of low-energy electrons (0–14 eV) in the gas phase. Upon a single electron attachment, eight anionic fragments are observed, the most intense being an anion with mass of 109 u at a resonance energy of 0 eV. Quantum chemical calculations suggest that this ion is generated after the tetrazine ring opens along a N–N bond and its fragments leave the molecule, forming an imidazole-carboxamide species. This ion represents the most abundant fragment, with further fragments following from its dissociation. The tetrazine ring cleavage reaction forming N_2 is thus the driving force of TMZ reactivity upon electron attachment.

Keywords: temozolomide, electron attachment, imidazole ring, gas phase, ring cleavage

OPEN ACCESS

Edited by:
Nigel John Mason, University of Kent, United Kingdom

Reviewed by:
Vitaly V. Kresin, University of Southern California, Los Angeles, United States
Aparna Shastri, Bhabha Atomic Research Centre (BARC), India

****Correspondence:***
Milan Ončák
milan.oncak@uibk.ac.at
Stephan Denifl
stephan.denifl@uibk.ac.at

Specialty section:
This article was submitted to Atomic and Molecular Physics, a section of the journal Frontiers in Physics

Received: *21 February 2022*
Accepted: *06 April 2022*
Published: *27 April 2022*

Citation:
Arthur-Baidoo E, Izadi F, Guerra C, Garcia G, Ončák M and Denifl S (2022) Dynamics of Ring-Cleavage Reactions in Temozolomide Induced by Low-Energy Electron Attachment. Front. Phys. 10:880689. doi: 10.3389/fphy.2022.880689

INTRODUCTION

Anticancer drugs have been used in the treatment of cancer most especially for combination therapy involving radiation therapy and concomitant chemotherapy [1]. Such drugs that enhance the efficacy of ionizing radiation during cancer treatment are often referred to as radiosensitizers. Several of them have been suggested, and they undergo further investigation for their effective use for therapy based on their function and the kind of tumour [2–5]. They include imidazoles, which consist of five-membered heterocyclic ring compounds with two nitrogen atoms, that have demonstrated efficacy in terms of their pharmaceutical activities and their use as anticancer agents [2, 6]. In addition, the fact that the imidazole ring is rich in electrons makes it easier for imidazole derivatives to bind to receptors and enzymes within a biological medium through hydrogen bonding, π–π stacking or van der Waals forces [6, 7]. Imidazoles are believed to interact with DNA in both covalent or non-covalent pathway and block cell division, easily bind to proteins and inhibit the synthesis of cellular membranes [2, 6, 7]. Chemical agents such as dacarbazin, nimorazole, mercaptopurine etc. used in the treatment of cancer contain the imidazole ring within the structure. For instance, dacarbazin acts as an alkylating agent that destroys cancer cells by the addition of an alkyl group to DNA [2]. Of the various imidazole ring containing compounds, the bicyclic aromatic heterocyclic derivative known as imidazotetrazines have gained attention because of the alkylating properties of its derivatives. The most prominent compound of these is temozolomide [8–10].

Temozolomide (3-methyl-4-oxoimidazo[5,1-d][1,2,3,5]tetrazine-8-carboxamide, TMZ) is a monofunctional alkylating and a prodrug that is known for its ability to surpass the blood-brain barrier [11–13]. TMZ is an imidazotetrazine derivative of dacarbazin and the 3-methyl derivative of the prodrug mitozolomide. The drug has shown a wide range of antineoplastic activity [13–16] and

cytotoxic activity in cell lines and on human tumors that were refractory to several clinically antitumor agents [14, 15, 17–19].

Regardless of the established biologically proposed mechanism of interaction, it is also relevant to understand the role of low energy electrons in the action of TMZ during its use in radiation therapy. In cancer treatment using ionizing radiation, the impact of such high-energy radiation with the biological medium produces a large number of secondary electrons (SEs) with kinetic energy between 0 and few hundreds of electron volts (eV) [20–22]. Of these SEs, low-energy electrons are the major contribution with energy below 20 eV and might cause single and double strand breaks in the DNA *via* site-selective bond cleavage [23, 24]. It is also known that the induction of these strand breaks depends on the initial kinetic energy of the electrons. Interestingly, these low-energy electrons have an average energy close to 9–10 eV [21, 22]. In studies of the condensed phase, it was shown that electrons with an energy as low as 0–4 eV have the propensity to induce single strand breaks in plasmid DNA [21, 22, 24]. At such low energies, it has been proven that dissociative electron attachment (DEA) represents the underlying mechanism in causing DNA damage by the formation of reactive species [25–27].

DEA involves the resonant capture of a single incoming electron by a molecule (AB) resulting in the initial formation of an intermediate derivative (AB^{*-}) known as the transient negative ion (TNI) [25, 28]. The TNI then decomposes into a negatively charged ion (B^-) and a neutral (A) as shown in reaction (1):

$$e^- + AB \rightarrow AB^{*-} \rightarrow A + B^- \quad (1)$$

Although thermodynamics and kinetics of isolated systems differ from that in the condensed phase due to the lack of molecular environment, gas phase studies have been instrumental in the study of the basic mechanisms of electron-molecule interactions at the molecular level. Several gas-phase studies on radiosensitizers have shown site-selective fragmentation upon electron attachment [29–33]. Often this behavior may result in the detection of the dehydrogenated parent anion $(M–H)^-$, which is one of the most prominent anions in DEA to molecules containing hydrogen(s) *via* single bond cleavage, with possible subsequent fragmentation [34, 35]. In addition, DEA studies with tirapazamine demonstrated that the attachment of a single electron could induce the formation of several ring-centered and N-centered fragments when the triazine ring opens [36].

To our knowledge, no DEA study with TMZ in the gas phase has been reported so far. Herein, we investigate DEA to TMZ in the gas phase within the electron energy range of 0–10 eV. The obtained experimental results are supported by quantum chemical calculation to rationalize the reaction dynamics and energetics of the involved channels.

METHODS

The experimental setup used for the present study was a crossed electron-molecular beam setup coupled with a quadrupole mass analyzer. Since a detailed description of the setup can be found in Ref. [37], only a brief summary in relation to the current study is given. Temozolomide ($C_6H_6N_6O_2$, 194 g/mol) with a sample purity of 98% was purchased from Sigma Aldrich, Austria, and used as delivered. In the powder state at room temperature, TMZ was placed in an oven. The sample was then heated to about 390 ± 3 K under high vacuum (10^{-7} mbar) and the vaporized sample was introduced into the interaction zone with the electron beam *via* a 1 mm capillary mounted on the oven. Thermal decomposition of the sample was ruled out by measuring the temperature dependence of the electron ionization mass spectrum of TMZ. The electron beam created by the hemispherical electron monochromator perpendicularly crosses the effusive molecular beam. Negatively charged ions formed by electron attachment are then extracted by a weak electrostatic field and directed towards the quadrupole mass analyser. After mass analysis, the ions are finally detected by a channel electron multiplier operating in single ion-counting mode. The energy scale of the monochromator was calibrated using the well-known s-wave resonance of carbon tetrachloride (CCl_4) at 0 eV. In the ideal case, the electron beam should be able to give an energy resolution of 35 meV. For this study and to keep a compromise between the signal intensity and resolution, we tune the beam to 100 meV at Full-Width-Half-Maximum (FWHM) at an electron current of 25 nA. We further performed energy scans in 0–14 eV with a scanning step width of 0.03 eV for each of the fragment detected upon DEA to TMZ.

Structures of the TMZ, $TMZ^-$and its fragments were optimized using density functional theory (DFT) employing the B3LYP functional along with the aug-cc-pVDZ basis set. To obtain more reliable electronic energies, the optimized structures were single-point re-calculated at the coupled cluster singles and doubles level, CCSD/aug-cc-pVDZ. The zero-point energy correction was used as calculated at the B3LYP/aug-cc-pVDZ level. To assess the influence of the DFT functional on reaction energies, we also used the ωB97XD functional [38] to calculate structures of TMZ, $TMZ^-$and the ions after dissociation of N_2 and/or $OCNCH_3$. The respective reaction energies evaluated at the CCSD//ωB97XD level differ from those at the CCSD//B3LYP level by less than 0.02 eV (employing consistently the aug-cc-pVDZ basis set). Electronically excited states were calculated using Equation of Motion–Coupled Clusters Singles and Double (EOM-CCSD) and Time-Dependent Density Functional Theory (TD-DFT) with the CAM-B3LYP functional, the energy difference for the first excited valence π^* state in TMZ^-between EOM-CCSD and CAM-B3LYP methods is 0.04 eV. Natural transition orbital (NTO) analysis [39] was used to assign the transition character. For modeling the dipole bound state, the aug-cc-pVDZ basis set was used for C, O and N, the aug-cc-pVTZ basis set for hydrogen atoms, along with additional two *s*, one *p* and one *d* functions on each H atom, with coefficients obtained as 1/3 of that of the most diffuse *s*, *p* and *d* functions in aug-cc-pVTZ. This basis set is further denoted as aug-cc-pVDZ(C,N,O)TZ(H)+. Wave function stabilization was performed prior to each DFT or CCSD calculation. Vibrational analysis was performed to confirm the local minimum or

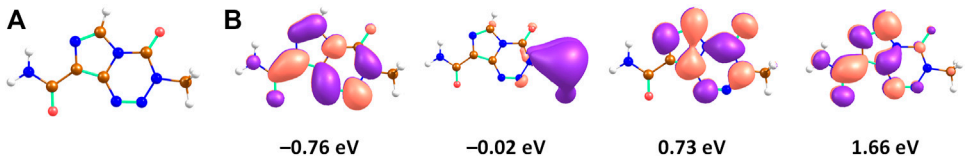

FIGURE 1 | (A) Structure of the TMZ molecule. **(B)** Orbitals occupied by a single electron in four TMZ^-electronic states in the optimal structure of the neutral molecule along with the relative energy compared to the neutral molecule; calculated at the CAM-B3LYP/aug-cc-pVDZ//B3LYP/aug-cc-pVDZ level of theory and shifted by the vertical electron affinity calculated at the CCSD/aug-cc-pVDZ level (0.76 eV). The orbitals were generated using natural transition orbitals analysis, the energy of the dipole-bound state was obtained using the aug-cc-pVDZ(C,N,O)TZ(H)$^+$ basis set, see Methods. Color code: brown–carbon, blue–nitrogen, red–oxygen, white–hydrogen.

TABLE 1 | Summary of fragment anions, structural assignments and their corresponding resonance positions, as well as experimental and calculated thresholds upon electron attachment to TMZ. Calculated thresholds were obtained at the CCSD/aug-cc-pVDZ//B3LYP/aug-cc-pVDZ level of theory.

Mass/u	Anion	Resonance positions/eV								Threshold/eV	
		1	2	3	4	5	6	7	8	Exp	Theo
137	$C_4H_3N_5O^-$	0	0.1	0.2	0.5	5.0	—	—	—	~0	–1.31
109	$C_4H_3N_3O^-$	0	0.1	0.2	0.4	0.9	2.8	—	—	~0	–1.41
91	$C_4HN_3^-$	0	0.3	0.9	2.4	4.1	—	—	—	~0	–0.88
82	$C_3H_2N_2O^-$	1.3	2.8	3.5	4.3	6.4	—	—	—	~0.8	–0.54
66	C_3NO^-	0	0.5	1.4	2.6	4.5	5.5			~0	–0.17
42	NCO^-	0	0.2	0.4	1.3	2.8	3.5	4.3	5.2	~0	–2.79
39	C_2HN^-	3.0	4.7	5.6	6.7		—	—	—	~2	1.43
26	CN^-	1.5	3.2	4.8	6.4	7.5	—	—	—	~1.7	1.99

transition state character of each calculated structure. The Gaussian software was used for all calculations [40].

RESULTS AND DISCUSSIONS

The structure of TMZ is shown in **Figure 1**, along with four electronic states of the TMZ^-anion. The adiabatic electron affinity is calculated as 1.28 eV, the vertical electron affinity as 0.76 eV at the CCSD/aug-cc-pVDZ//B3LYP/aug-cc-pVDZ level (with B3LYP/aug-cc-pVDZ and ωB97XD/aug-cc-pVDZ methods, we obtained the vertical electron affinity of 1.03 and 0.89 eV, respectively, indicating that these functionals overestimate the electron binding energy). In the structure of the neutral TMZ molecule, there is only one electronic state of TMZ^-below the energy of the neutral molecule, with the odd electron in a π^* orbital extended over both rings (**Figure 1**). The orbital hints towards weakening of the tetrazine ring, among others along a N–N bond. Close to the energy of the neutral molecule, a dipole-bound state (DBS) is found, with the added electron positioned next to the methyl group on the tetrazine ring (the dipole moment of the TMZ isomer shown in **Figure 1** is calculated as 3.4 Debye). Further two valence states lie within 2 eV above the energy of the neutral molecule, again with the odd electron in a π^* orbital, located predominantly on either triazine or imidazole ring. The analyzed electronic states thus suggest that a DBS might be formed after interaction with electrons of the kinetic energy close to 0 eV, serving as a doorway to the valence ground state, a process commonly suggested in DEA of polar molecules [41]. However, further experiments would be needed to confirm this scenario, e.g., photoelectron spectroscopy [42, 43].

Experimentally, electron attachment to TMZ in the gas phase resulted in the formation of eight anion fragments that arise due to multiple bond cleavage within the molecule and re-arrangement. A summary of the resonances and anions detected is presented in **Table 1**. It is interesting to mention that we do not observe formation of the parent anion or the dehydrogenated parent anion as observed in most DEA studies with other radiosensitizers and modified derivatives [44–47]. The absence of the parent anion can be traced to efficient dissociation reactions in the TNI, as discussed below.

The outcome of DEA to TMZ can be divided into three groups with respect to the fragmentation behavior of the TNI: 1) Anions resulting from the initial decomposition of the tetrazine ring and ring-containing anions, 2) anions resulting from the rupture of the imidazole ring, and 3) pseudohalogen anions.

Figure 2A shows the anion yield curve for mass of 137 u assigned as $C_4H_3N_5O^-$. In the absence of the parent anion or the dehydrogenated parent anion, we observe this anion as the heaviest one. Further, we observe the anion with mass of 109 u, which we assign as $C_4H_3N_3O^-$ (**Figure 2B**). This anion is the most abundant fragment with an ion yield of two to four orders of magnitude higher in abundance than for all other anions. Both anions show a prominent peak at ~0 eV. For the ion at 137 u, the data suggest a second resonance, although low in intensity, between 4 and 6 eV with a peak maximum around 5 eV. For the ion with mass of 109 u, resonances with maxima near 0.3 and 1 eV are observed as well.

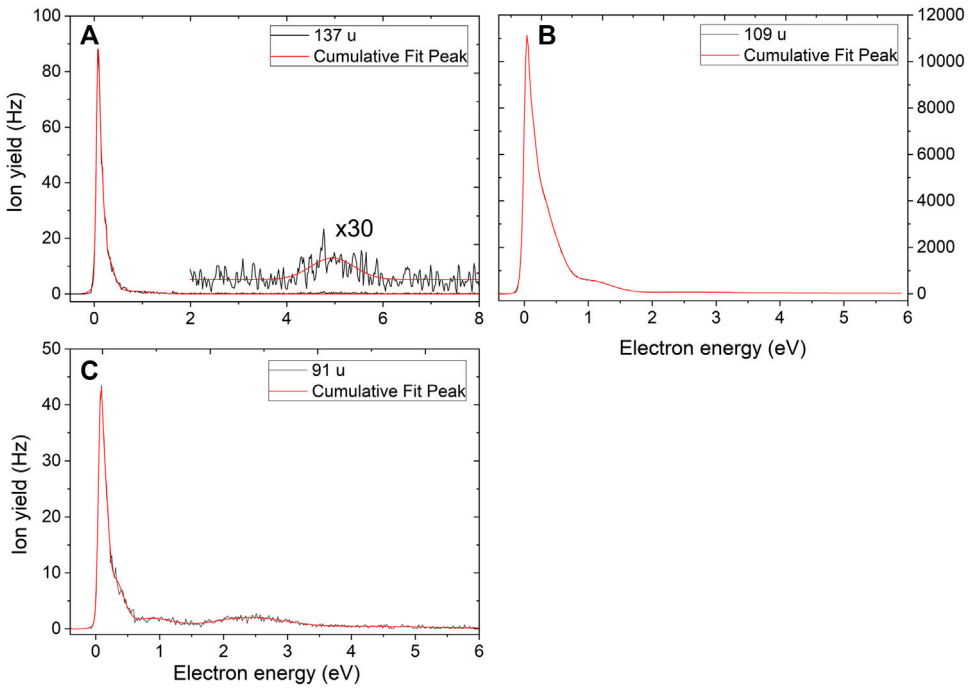

FIGURE 2 | (A–C) Anion efficiency curves for the anions with masses 137, 109 and 91 u formed upon electron attachment to TMZ, respectively.

The pathways to form the anionic fragments are analyzed in **Figure 3**, assuming that the anion reaches its ground state after electron attachment. Formation of both 137 u and 109 u ions may be associated with opening of the tetrazine ring at a N–N bond over a barrier with the energy of –0.78 eV with respect to the neutral TMZ molecule. From this structure, $OCNCH_3$ or N_2 fragments might dissociate. If $OCNCH_3$ dissociates, the ion with mass of 137 u is formed. If the $OCNCH_3$ fragment takes away enough kinetic energy, this anion cannot decompose further and is observed in the experiment. Otherwise, the ion might lose N_2 in an exothermic reaction, proceeding over a barrier at –0.81 eV (not shown in **Figure 3**). The other pathway starts with dissociation of N_2, forming an anion with 166 u at –1.98 eV. This ion is not observed experimentally, probably because it further dissociates $OCNCH_3$ or undergoes other dissociation reactions.

If both $OCNCH_3$ are N_2 are released from the cluster, an ion with 109 u is formed. Here, the tetrazine ring is dissociated completely and only the substituted imidazole ring is left. The ion can decompose only through reactions that require considerable bond rearrangement, explaining its stability in the experiment. Accordingly, we suggest that this ion plays a pivotal role in further cluster dissociation as discussed below.

Figure 3 also includes the length of a C–N bond in the imidazole ring as well as of the N–N bond of the forming N_2 molecule. It can be seen that both bond lengths decrease considerably along the dissociation pathway, rationalizing the increased stability of the structures with a cleaved ring compared to the initial anion. For example, the N–N bond length starts with 1.33 Å in the intact anion and decreases to 1.19 Å upon ring opening and to 1.10 Å when dissociated as N_2, strengthening the bond along the dissociation pathway.

The anion efficiency curve for the anion with mass 91 u is shown in **Figure 2C**. The ion yield shows three visible resonance maxima comprising of a sharp peak at ~0 eV and two broad but low-intensity peaks near 0.9 and 2.4 eV. In addition, we suggest the existence of another peak below 1 eV due to the tail of the 0 eV peak. We assign the ion yield to the $C_4HN_3^-$ fragment anion and suggest that it could be formed through formation of two O–H bonds and H_2O loss from the $C_4H_3N_3O^-$anion, with the overall reaction energy of –0.88 eV (**Figure 3**). In agreement with the low experimental yield, our calculations show that already the first reaction step, i.e. formation of an OH group, proceeds over a transition states at 0.42 eV, close to the average thermal energy available in TMZ at 390 K, 0.52 eV.

Thus, all three ions $C_4H_3N_5O^-$, $C_4H_3N_3O^-$and $C_4HN_3^-$ are connected in their dissociation pathways and possess an intact imidazole ring. This assignment is supported by the fact that they share the characteristic resonance at ~0 eV.

Dissociation of the imidazole-carboxamide structure with mass 109 u gives rise to further four anionic fragments *via* multiple bond cleavages. The resulting fragments include anions with masses 82, 66, 39, and 26 u (**Figure 3**). The anion with mass 82 u may arise *via* the release of hydrogen cyanide (HCN) forming the structure $C_3H_2N_2O^-$, with the predicted reaction energy of –0.54 eV. The anion efficiency curve (**Figure 4A**) shows several peak positions. Since the tiny signal close to ~0 eV may also represent an artifact, we estimate the experimental threshold to be 0.8 eV with the peak maximum near 1.3 eV. Furthermore, the remaining resonances

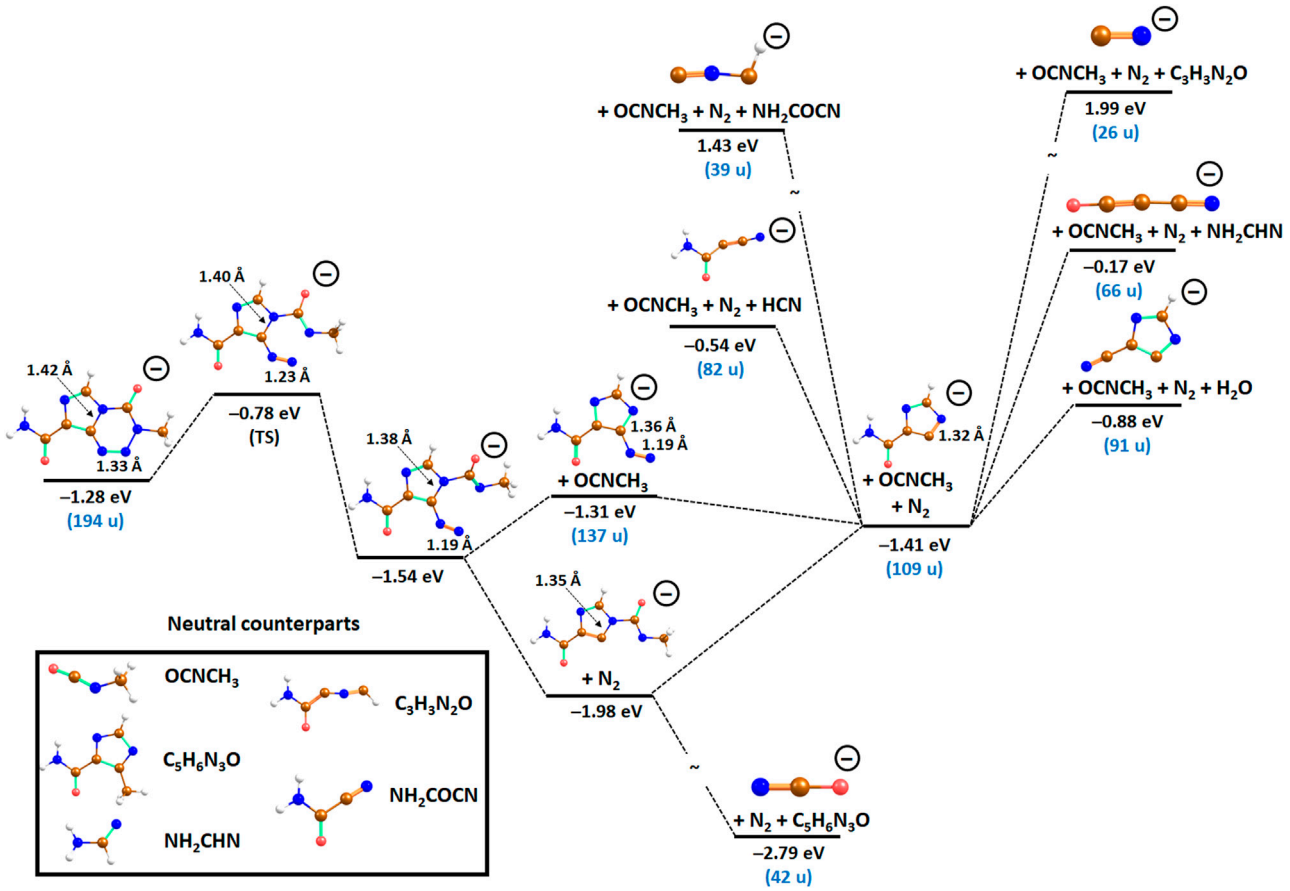

FIGURE 3 | Suggested reaction pathways in TMZ^- as analyzed at the CCSD/aug-cc-pVDZ//B3LYP/aug-cc-pVDZ level along with selected bond lengths. Mass is shown for the parent anion and experimentally observed fragments. Color code: brown–carbon, blue–nitrogen, red–oxygen, white–hydrogen.

appear at an electron energy of 2.8, 3.5, and 4.3 eV, and there is a peak near 6.4 eV close to the tail.

We assign the anion with mass 66 u to C_3NO^- (**Figure 4B**). The experimental threshold of ~0 eV agrees with the theoretically determined threshold of –0.17 eV. We observe three regions of resonances that comprise the region between 0 and 1, 1–2 eV, and 2–8 eV. The first region shows a rather sharp peak at ~0 eV and another one at 0.5 eV. The second peak section shows a single peak maximum at 1.4 eV. The third set of resonances is found at the maxima of 2.6 and 4.5 eV. In addition, another resonance is observed around 5.5 eV, close to the tail of the curve. At the B3LYP/aug-cc-pVDZ level, the C_3NO^- structure is predicted to be almost linear.

The anion with mass 42 u is assigned as NCO^- following multiple bond cleavage within the TMZ^- anion. Its anion efficiency curve (**Figure 4C**) shows several peak positions. For the first resonance, we observed a sharp peak maximum at ~0 eV and other minor features along the tail. The second distinct peak is observed with a maximum of 1.3 eV, an intense peak is seen at the resonance energy of 2.8 eV, followed by a shoulder exhibiting a resonance around 4.3 eV. The NCO^- anion appeared as the second most abundant one among all fragments.

The formation of the pseudohalogen NCO^- has been extensively reported in several DEA studies involving nucleobases [29, 48–50]. It was reported that its formation follows a complex unimolecular pathway that occurs on a longer time scale than for simple bond cleavage [49]. The pathway starts in nucleobases by bond cleavage leading to the loss of a hydrogen atom and subsequent multiple bond cleavage within the ring [49]. In DEA to TMZ, its formation may be expected at different sites. In **Figure 3**, we suggest that it might arise from TMZ^- upon N_2 dissociation followed by CH_3 transfer from the dissociating $OCNCH_3$ fragment to the imidazole ring, reaching the reaction energy of –2.79 eV. The considerable experimental intensity may be thus rationalized by its thermochemical stability. This may be the main reason why it is a common, intense product anion in DEA to NCO-containing molecules and often formed in a wide range of electron energies [29, 35, 51].

Another fragment anion forming after the imidazole ring opens is the anion with mass 39 u, which may be assigned as C_2HN^-. The formation of the anion follows the reaction releasing NH_2COCN from $C_4H_3N_3O^-$ as the neutral counterpart, with the calculated threshold of 1.43 eV, which is below the experimental onset of ~2 eV. The anion efficiency curve in **Figure 4D** exhibits a peak maximum at 4.7 eV and other subjacent features in the tail around

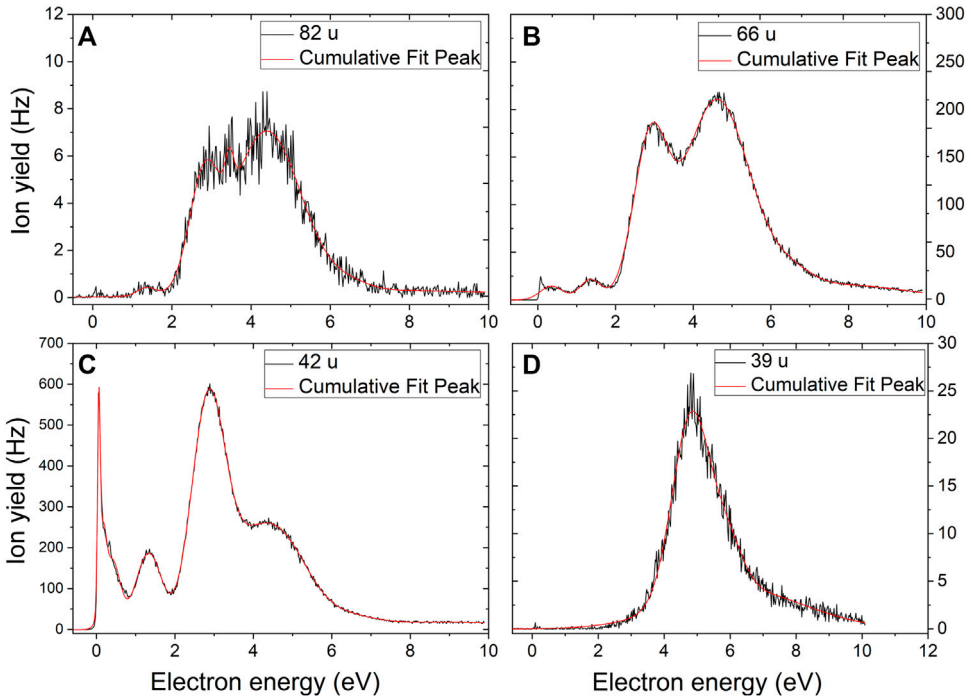

FIGURE 4 | (A–D) Anion efficiency curves for the anions with masses 82, 66, 42 and 39 u formed upon electron attachment to TMZ, respectively.

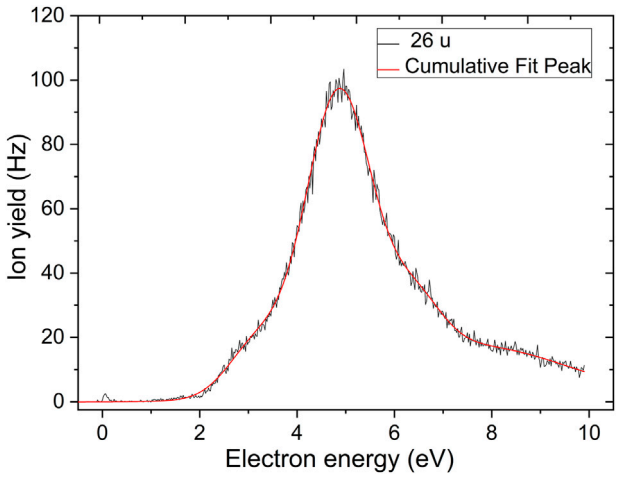

FIGURE 5 | Anion efficiency curve for CN^- formed upon electron attachment to TMZ.

5.6 and 6.7 eV. We also suggest a possible resonance near 3.0 eV close to the onset of the curve.

Finally, we also observed the pseudohalogen CN^- anion. The formation of CN^- has been reported in many DEA studies involving imidazole compounds [52, 53], amino compounds [54–56], heterocyclic compound [36] and uracil derivatives [32, 49, 57, 58]. Mostly, the anion is formed following a complete rupture of the ring in a molecule. Recent studies with molecules such as cyanamide, nitrofuran, and nicotinamide reported several resonances at electron energies above 1 eV for this pathway [36, 37, 59, 60]. An exceptional case was reported by Koenig-Lehmann et al. [51] in electron attachment studies with dibromocyanoacetamide, where the authors found an enormous signal close to 0 eV. In the present study, the formation of CN^- follows multiple bond cleavages within the imidazole-carboxamide derivative as shown in **Figure 3**. The anion efficiency curve indicates a major peak near 4.8 eV and three other resonances at 3.2, 6.4 and 7.5 eV (**Figure 5**). Our calculations predict an endothermic reaction with the energy of 1.99 eV, close to the experimental threshold of ~1.7 eV. However, we note that the CN^- anion might also form from several other sites. The 0 eV peak can be considered an artefact.

It is interesting to note that besides NCO^-, also the other four anions with lower masses (82, 66, 39 and 26 u) exhibit anion efficiency curves which are dominated by higher-energy resonances. This characteristic can be attributed to the large amount of energy required to rupture the imidazole ring. The similarity of certain peak regions, for example the peculiar resonance seen at 4–6 eV, also suggest that all anions arise from the same precursor, in agreement with the suggested pathways in **Figure 3**.

CONCLUSION

The present results suggest that the imidazole moiety is more stable upon low-energy electron attachment than the triazine moiety. A recent DEA study with tirapazamine (composed of

triazine and benzene moiety) also indicated the triazine moiety as a less stable moiety since the integrity of the benzene ring was preserved in the DEA reactions obtained [36]. On the other hand, molecular rearrangement and formation of new bonds act as an energy source and the presence of a triazine ring thus allows for DEA reactions to be induced by electrons having very low kinetic energies near zero eV. In contrast, the yields of anions which are formed by cleavage of the imidazole ring exhibit the main resonances only at higher electron energies. Such characteristics were observed in DEA to the isolated imidazole ring as well [61, 62] and seem to be preserved for bicyclic molecules.

DATA AVAILABILITY STATEMENT

The original contributions presented in the study are included in the article/**Supplementary Material**, further inquiries can be directed to the corresponding authors.

AUTHOR CONTRIBUTIONS

EA-B: Suggestion of compound, measurements, data analysis, preparation of first draft. FI: Measurements, data analysis, editing manuscript draft. CG: Measurements, editing manuscript draft. GG: Conception of study, funding, editing manuscript draft. MO: Quantum chemical calculations, preparation of first draft. SD: Conception and design of study, funding, interpretion of data, editing manuscript draft.

FUNDING

SD acknowledges funding support by the Austrian Science Fund (FWF), Vienna (P30332). The computational results presented have been achieved using the HPC infrastructure LEO of the University of Innsbruck. CG and GG acknowledge partial financial support from the Spanish Ministerio de Ciencia e Innovación (Project PID2019-104727RB-C21) and CSIC (Project LINKA20085).

SUPPLEMENTARY MATERIAL

The Supplementary Material for this article can be found online at: https://www.frontiersin.org/articles/10.3389/fphy.2022.880689/full#supplementary-material

REFERENCES

1. Wang H, Mu X, He H, Zhang X-D. Cancer Radiosensitizers. *Trends Pharmacol Sci* (2018) 39:24–48. doi:10.1016/j.tips.2017.11.003
2. Ali I, Lone MN, Aboul-Enein HY. Imidazoles as Potential Anticancer Agents. *Med Chem Commun* (2017) 8:1742–73. doi:10.1039/C7MD00067G
3. Wardman P. Chemical Radiosensitizers for Use in Radiotherapy. *Clin Oncol* (2007) 19:397–417. doi:10.1016/j.clon.2007.03.010
4. Oronsky B, Scicinski J, Ning S, Peehl D, Oronsky A, Cabrales P, et al. RRx-001, A Novel Dinitroazetidine Radiosensitizer. *Invest New Drugs* (2016) 34:371–7. doi:10.1007/s10637-016-0326-y
5. Ning S, Bednarski M, Oronsky B, Scicinski J, Saul G, Knox SJ. Dinitroazetidines Are a Novel Class of Anticancer Agents and Hypoxia-Activated Radiation Sensitizers Developed from Highly Energetic Materials. *Cancer Res* (2012) 72:2600–8. doi:10.1158/0008-5472.CAN-11-2303
6. Sharma P, LaRosa C, Antwi J, Govindarajan R, Werbovetz KA. Imidazoles as Potential Anticancer Agents: An Update on Recent Studies. *Molecules* (2021) 26:4213. doi:10.3390/molecules26144213
7. Zhang L, Peng X-M, Damu GLV, Geng R-X, Zhou C-H. Comprehensive Review in Current Developments of Imidazole-Based Medicinal Chemistry. *Med Res Rev* (2014) 34:340–437. doi:10.1002/med.21290
8. Svec RL, McKee SA, Berry MR, Kelly AM, Fan TM, Hergenrother PJ. Novel Imidazotetrazine Evades Known Resistance Mechanisms and Is Effective against Temozolomide-Resistant Brain Cancer in Cell Culture. *ACS Chem Biol* (2022) 17:299–313. doi:10.1021/acschembio.2c00022
9. Bouzinab K, Summers H, Zhang J, Stevens MFG, Moody CJ, Turyanska L, et al. In Search of Effective Therapies to Overcome Resistance to Temozolomide in Brain Tumours. *Cdr* (2019) 2:1018–31. doi:10.20517/cdr.2019.64
10. Svec RL, Hergenrother PJ. Imidazotetrazines as Weighable Diazomethane Surrogates for Esterifications and Cyclopropanations. *Angew Chem* (2020) 132:1873–8. doi:10.1002/ange.201911896
11. Newlands ES, Stevens MFG, Wedge SR, Wheelhouse RT, Brock C. Temozolomide: A Review of its Discovery, Chemical Properties, Pre-clinical Development and Clinical Trials. *Cancer Treat Rev* (1997) 23:35–61. doi:10.1016/S0305-7372(97)90019-0
12. Syro LV, Ortiz LD, Scheithauer BW, Lloyd R, Lau Q, Gonzalez R, et al. Treatment of Pituitary Neoplasms with Temozolomide. *Cancer* (2011) 117:454–62. doi:10.1002/cncr.25413
13. Thomas A, Tanaka M, Trepel J, Reinhold WC, Rajapakse VN, Pommier Y. Temozolomide in the Era of Precision Medicine. *Cancer Res* (2017) 77:823–6. doi:10.1158/0008-5472.CAN-16-2983
14. Lee SY. Temozolomide Resistance in Glioblastoma Multiforme. *Genes Dis* (2016) 3:198–210. doi:10.1016/j.gendis.2016.04.007
15. Darkes MJM, Plosker GL, Jarvis B, Atri SD, Dermopatico I, Immacolata D, et al. Temozolomide. *Am J Cancer* (2002) 1:55–80. doi:10.2165/00024669-200201010-00006
16. Moody C, Wheelhouse R. The Medicinal Chemistry of Imidazotetrazine Prodrugs. *Pharmaceuticals* (2014) 7:797–838. doi:10.3390/ph7070797
17. Grossman SA, Ye X, Piantadosi S, Desideri S, Nabors LB, Rosenfeld M, et al. Survival of Patients with Newly Diagnosed Glioblastoma Treated with Radiation and Temozolomide in Research Studies in the United States. *Clin Cancer Res* (2010) 16:2443–9. doi:10.1158/1078-0432.CCR-09-3106
18. Friedman HS, Kerby T, Calvert H. Temozolomide and Treatment of Malignant Glioma. *Clin Cancer Res* (2000) 6:2585–97.
19. Sperry JB, Stone S, Azuma M, Barrett C. Importance of Thermal Stability Data to Avoid Dangerous Reagents: Temozolomide Case Study. *Org Process Res Dev* (2021) 25:1690–700. doi:10.1021/acs.oprd.1c00206
20. Gao Y, Zheng Y, Sanche L. Low-Energy Electron Damage to Condensed-phase DNA and its Constituents. *Ijms* (2021) 22:7879. doi:10.3390/ijms22157879
21. Pimblott SM, LaVerne JA. Production of Low-Energy Electrons by Ionizing Radiation. *Radiat Phys Chem* (2007) 76:1244–7. doi:10.1016/j.radphyschem.2007.02.012
22. LaVerne JA, Pimblott SM. Electron Energy-Loss Distributions in Solid, Dry DNA. *Radiat Res* (1995) 141:208–15. doi:10.2307/3579049
23. Baccarelli I, Bald I, Gianturco FA, Illenberger E, Kopyra J. Electron-Induced Damage of DNA and its Components: Experiments and Theoretical Models. *Phys Rep* (2011) 508:1–44. doi:10.1016/j.physrep.2011.06.004

24. Boudaiffa B, Cloutier P, Hunting D, Huels MA, Sanche L. Resonant Formation of DNA Strand Breaks by Low-Energy (3 to 20 eV) Electrons. *Science* (2000) 287:1658–60. doi:10.1126/science.287.5458.1658
25. Bald I, Langer J, Tegeder P, Ingólfsson O. From Isolated Molecules through Clusters and Condensates to the Building Blocks of Life. *Int J Mass Spectrom* (2008) 277:4–25. doi:10.1016/j.ijms.2008.06.013
26. Arthur-Baidoo E, Ameixa J, Ziegler P, Ferreira da Silva F, Ončák M, Denifl S. Reactions in Tirapazamine Induced by the Attachment of Low-Energy Electrons: Dissociation versus Roaming of OH. *Angew Chem Int Ed* (2020) 59:17177–81. doi:10.1002/anie.202006675
27. Ptasińska S, Alizadeh E, Sulzer P, Abouaf R, Mason NJ, Märk TD, et al. Negative Ion Formation by Low Energy Electron Attachment to Gas-phase 5-Nitrouracil. *Int J Mass Spectrom* (2008) 277:291–5. doi:10.1016/j.ijms.2008.06.008
28. Dawley MM, Tanzer K, Carmichael I, Denifl S, Ptasińska S. Dissociative Electron Attachment to the Gas-phase Nucleobase Hypoxanthine. *J Chem Phys* (2015) 142:215101. doi:10.1063/1.4921388
29. Denifl S, Matejcik S, Gstir B, Hanel G, Probst M, Scheier P, et al. Electron Attachment to 5-Chloro Uracil. *J Chem Phys* (2003) 118:4107–14. doi:10.1063/1.1540108
30. Denifl S, Ptasińska S, Hanel G, Gstir B, Probst M, Scheier P, et al. Electron Attachment to Gas-phase Uracil. *J Chem Phys* (2004) 120:6557–65. doi:10.1063/1.1649724
31. Sulzer P, Ptasinska S, Zappa F, Mielewska B, Milosavljevic AR, Scheier P, et al. Dissociative Electron Attachment to Furan, Tetrahydrofuran, and Fructose. *J Chem Phys* (2006) 125:044304. doi:10.1063/1.2222370
32. Meißner R, Makurat S, Kozak W, Limão-Vieira P, Rak J, Denifl S. Electron-Induced Dissociation of the Potential Radiosensitizer 5-Selenocyanato-2′-Deoxyuridine. *J Phys Chem B* (2019) 123:1274–82. doi:10.1021/acs.jpcb.8b11523
33. Ptasińska S, Denifl S, Scheier P, Märk TD. Inelastic Electron Interaction (Attachment/Ionization) with Deoxyribose. *J Chem Phys* (2004) 120:8505–11. doi:10.1063/1.1690231
34. Gschliesser D, Vizcaino V, Probst M, Scheier P, Denifl S. Formation and Decay of the Dehydrogenated Parent Anion upon Electron Attachment to Dialanine. *Chem Eur J* (2012) 18:4613–9. doi:10.1002/chem.201102433
35. Huber SE, Śmiałek MA, Tanzer K, Denifl S. Dissociative Electron Attachment to the Radiosensitizing Chemotherapeutic Agent Hydroxyurea. *J Chem Phys* (2016) 144:224309. doi:10.1063/1.4953579
36. Arthur-Baidoo E, Ameixa J, Ončák M, Denifl S. Ring-Selective Fragmentation in the Tirapazamine Molecule upon Low-Energy Electron Attachment. *Ijms* (2021) 22:3159. doi:10.3390/ijms22063159
37. Saqib M, Arthur-Baidoo E, Ončák M, Denifl S. Electron Attachment Studies with the Potential Radiosensitizer 2-Nitrofuran. *Ijms* (2020) 21:8906. doi:10.3390/ijms21238906
38. Chai J-D, Head-Gordon M. Long-range Corrected Hybrid Density Functionals with Damped Atom-Atom Dispersion Corrections. *Phys Chem Chem Phys* (2008) 10:6615–20. doi:10.1039/b810189b
39. Martin RL. Natural Transition Orbitals. *J Chem Phys* (2003) 118:4775–7. doi:10.1063/1.1558471
40. Frisch MJ, Trucks GW, Schlegel HB, Scuseria GE, Robb MA, Cheeseman JR, et al. *Gaussian 16 Revision a. 03. 2016*. Wallingford CT: Gaussian Inc. (2016). p. 2.
41. Sommerfeld T. Dipole-Bound States as Doorways in (Dissociative) Electron Attachment. *Proc J Phys Conf Ser* (2005) 4:36. doi:10.1088/1742-6596/4/1/036
42. Ciborowski SM, Liu G, Graham JD, Buytendyk AM, Bowen KH. Dipole-Bound Anions: Formed by Rydberg Electron Transfer (RET) and Studied by Velocity Map Imaging--Anion Photoelectron Spectroscopy (VMI--APES). *Eur Phys J D* (2018) 72:1–5. doi:10.1140/epjd/e2018-90182-y
43. Castellani ME, Anstöter CS, Verlet JRR. On the Stability of a Dipole-Bound State in the Presence of a Molecule. *Phys Chem Chem Phys* (2019) 21:24286–90. doi:10.1039/c9cp04942h
44. Ameixa J, Arthur-Baidoo E, Meißner R, Makurat S, Kozak W, Butowska K, et al. Low-Energy Electron-Induced Decomposition of 5-Trifluoromethanesulfonyl-Uracil: A Potential Radiosensitizer. *J Chem Phys* (2018) 149:164307. doi:10.1063/1.5050594
45. Spisz P, Zdrowowicz M, Kozak W, Chomicz-Mańka L, Falkiewicz K, Makurat S, et al. Uracil-5-yl O-Sulfamate: An Illusive Radiosensitizer. Pitfalls in Modeling the Radiosensitizing Derivatives of Nucleobases. *J Phys Chem B* (2020) 124:5600–13. doi:10.1021/acs.jpcb.0c03844
46. Kopyra J, Keller A, Bald I. On the Role of Fluoro-Substituted Nucleosides in DNA Radiosensitization for Tumor Radiation Therapy. *RSC Adv* (2014) 4:6825–9. doi:10.1039/c3ra46735j
47. Meißner R, Feketeová L, Illenberger E, Denifl S. Reactions in the Radiosensitizer Misonidazole Induced by Low-Energy (0-10 eV) Electrons. *Ijms* (2019) 20:3496. doi:10.3390/ijms20143496
48. Burrow PD, Gallup GA, Scheer AM, Denifl S, Ptasinska S, Märk T, et al. Vibrational Feshbach Resonances in Uracil and Thymine. *J Chem Phys* (2006) 124:124310. doi:10.1063/1.2181570
49. Da Silva FF, Matias C, Almeida D, García G, Ingólfsson O, Flosadóttir HD, et al. NCO-, a Key Fragment upon Dissociative Electron Attachment and Electron Transfer to Pyrimidine Bases: Site Selectivity for a Slow Decay Process. *J Am Soc Mass Spectrom* (2013) 24:1787–97. doi:10.1007/s13361-013-0715-9
50. Abdoul-Carime H, Huels MA, Illenberger E, Sanche L. Formation of Negative Ions from Gas Phase Halo-Uracils by Low-Energy (0-18 eV) Electron Impact. *Int J Mass Spectrom* (2003) 228:703–16. doi:10.1016/S1387-3806(03)00139-8
51. Koenig-Lehmann C, Kopyra J, Dąbkowska I, Kočišek J, Illenberger E. Excision of CN– and OCN– from Acetamide and Some Amide Derivatives Triggered by Low Energy Electrons. *Phys Chem Chem Phys* (2008) 10:6954–61. doi:10.1039/B812130C
52. Meißner R, Feketeová L, Bayer A, Limão-Vieira P, Denifl S. Formation of Negative and Positive Ions in the Radiosensitizer Nimorazole upon Low-Energy Electron Collisions. *J Chem Phys* (2021) 154:074306. doi:10.1063/5.0040045
53. Tanzer K, Feketeová L, Puschnigg B, Scheier P, Illenberger E, Denifl S. Reactions in Nitroimidazole and Methylnitroimidazole Triggered by Low-Energy (0-8 eV) Electrons. *J Phys Chem A* (2015) 119:6668–75. doi:10.1021/acs.jpca.5b02721
54. Alizadeh E, Gschliesser D, Bartl P, Hager M, Edtbauer A, Vizcaino V, et al. Bond Dissociation of the Dipeptide Dialanine and its Derivative Alanine Anhydride Induced by Low Energy Electrons. *J Chem Phys* (2011) 134:054305. doi:10.1063/1.3544217
55. Denifl S, Flosadóttir HD, Edtbauer A, Ingólfsson O, Märk TD, Scheier P. A Detailed Study on the Decomposition Pathways of the Amino Acid Valine upon Dissociative Electron Attachment. *Eur Phys J D* (2010) 60:37–44. doi:10.1140/epjd/e2010-00060-5
56. Ziegler P, Pelc A, Arthur-Baidoo E, Ameixa J, Ončák M, Denifl S. Negative Ion Formation and Fragmentation upon Dissociative Electron Attachment to the Nicotinamide Molecule. *RSC Adv* (2021) 11:32425–34. doi:10.1039/d1ra06083j
57. Hanel G, Gstir B, Denifl S, Scheier P, Probst M, Farizon B, et al. Electron Attachment to Uracil: Effective Destruction at Subexcitation Energies. *Phys Rev Lett* (2003) 90:188104. doi:10.1103/PhysRevLett.90.188104
58. Arthur-Baidoo E, Falkiewicz K, Chomicz-Mańka L, Czaja A, Demkowicz S, Biernacki K, et al. Electron-Induced Decomposition of Uracil-5-yl O-(N,N-dimethylsulfamate): Role of Methylation in Molecular Stability. *Ijms* (2021) 22:2344. doi:10.3390/ijms22052344
59. Pelc A, Huber SE, Matias C, Czupyt Z, Denifl S. Formation of Negative Ions upon Dissociative Electron Attachment to the Astrochemically Relevant Molecule Aminoacetonitrile. *J Phys Chem A* (2016) 120:903–10. doi:10.1021/acs.jpca.5b09657
60. Tanzer K, Pelc A, Huber SE, Czupyt Z, Denifl S. Low Energy Electron Attachment to Cyanamide (NH_2CN). *J Chem Phys* (2015) 142:034301. doi:10.1063/1.4905500
61. Ribar A, Fink K, Li Z, Ptasińska S, Carmichael I, Feketeová L, et al. Stripping off Hydrogens in Imidazole Triggered by the Attachment of a Single Electron. *Phys Chem Chem Phys* (2017) 19:6406–15. doi:10.1039/C6CP08773F

62. Pshenichnyuk SA, Fabrikant II, Modelli A, Ptasińska S, Komolov AS. Resonance Electron Interaction with Five-Membered Heterocyclic Compounds: Vibrational Feshbach Resonances and Hydrogen-Atom Stripping. *Phys Rev A* (2019) 100:12708. doi:10.1103/PhysRevA.100.012708

Conflict of Interest: The authors declare that the research was conducted in the absence of any commercial or financial relationships that could be construed as a potential conflict of interest.

Publisher's Note: All claims expressed in this article are solely those of the authors and do not necessarily represent those of their affiliated organizations, or those of the publisher, the editors and the reviewers. Any product that may be evaluated in this article, or claim that may be made by its manufacturer, is not guaranteed or endorsed by the publisher.